Journal of Hazardous Materials 506 (2026) 141592

Contents lists available at ScienceDirect

Journal of Hazardous Materials

journal homepage: www.elsevier.com/locate/jhazmat

π-conjugated microplastics act as hazard amplifiers of antibiotic resistance through cross-kingdom network engineering

Tongyi Yang [a], Ruiqian Yuan [a], Xiujie Wang [a], Linzhi Zhai [a], Xiaona Dong [a], Haifeng Chen [a], Zechong Guo [a], Huazhe Jiao [b], Li-zhi Huang [c], Yixuan Yang [b,*], Qian-qian Jia [a,*]

[a] School of Environmental and Chemical Engineering, Jiangsu University of Science and Technology, Zhenjiang 212003, PR China
[b] School of Civil Engineering, Henan Polytechnic University, Jiaozuo 454003, PR China
[c] School of Civil Engineering, Wuhan University, No. 8, East Lake South Road, Wuhan, PR China

HIGHLIGHT

- π-Conjugated microplastics act as chemical hazard amplifiers via π–π stacking.
- Polystyrene-indole synergy chemically reprograms soil organic matter.
- Amplified indole signal dominates ARG spread (β=0.47, 23.5 × polymer effect).
- The fungus *Pseudeurotium* is a keystone hub bridging signal and ARG dissemination.
- The Chemical Interfacial-Driven Network Engineering (CIDNE) framework is introduced.

GRAPHICAL ABSTRACT

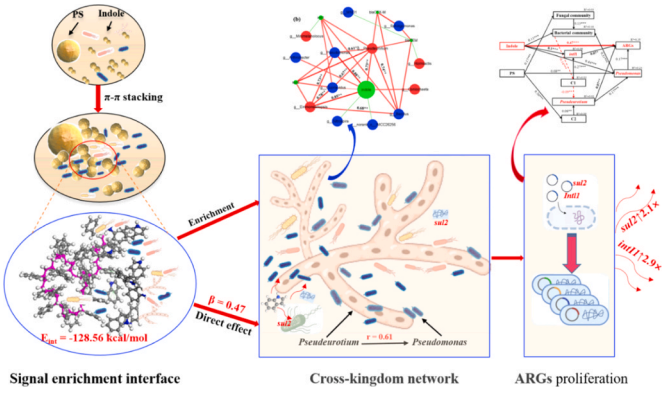

ARTICLE INFO

Keywords:
Antibiotic resistance genes
Chemical interfacial engineering
π-conjugated pollutants
Signal amplification
Cross-kingdom interactions

ABSTRACT

Microplastics are recognized as environmental vectors for antibiotic resistance genes (ARGs), a role traditionally ascribed to physical mechanisms such as biofilm-enhanced horizontal gene transfer. Here, we uncover a chemistry-driven pathway that fundamentally surpasses the traditional passive vector model. We show that π-conjugated polystyrene (PS) microplastics serve as powerful chemical hazard amplifyers by specifically concentrating the signaling molecule indole on their surfaces through π-π stacking and electrostatic interactions (binding energy = −128.56 kcal/mol), creating localized interfacial risk hotspots. These hotspots drive the reprogramming of soil microbiomes, as evidenced by distinct transformations in dissolved organic matter (DOM), and promote a cross-kingdom microbial alliance centered on the keystone fungus *Pseudeurotium*. This fungal hub transmits the amplified indole signal to bacterial degraders, markedly elevating the dissemination risk of clinically relevant ARGs (e.g., *sul2*). Through an integration of molecular simulations, multi-omics analyses, and causal modeling, our structural equation modeling (SEM) identifies the amplified indole signal as the primary direct driver of ARG abundance (path coefficient β = 0.47)—an effect 23.5 times greater than that of the PS polymer itself. Our findings establish "Chemical Interfacial-Driven Network Engineering (CIDNE)" as a pivotal

* Corresponding authors.
E-mail addresses: 490608791@qq.com (Y. Yang), qqj320@just.edu.cn (Q.-q. Jia).

https://doi.org/10.1016/j.jhazmat.2026.141592
Received 27 November 2025; Received in revised form 1 February 2026; Accepted 22 February 2026
Available online 23 February 2026

mechanism, redefining how synthetic materials actively reshape microbial networks and escalate environmental resistome risk through molecular-scale interfacial interactions.

1. Introduction

Antimicrobial resistance (AMR) is projected to cause 10 million deaths annually by 2050, with environmental reservoirs serving as critical crucibles for the evolution of resistance [1–3]. Current risk assessment paradigms typically view microplastics (MPs) as passive carriers of antibiotic resistance genes (ARGs) via biofilm-assisted horizontal gene transfer and plasmid exchange [4–6]. However, emerging research reveals that the sorption behavior of MPs is fundamentally governed by their surface chemistry and molecular structure, a property with profound implications for environmental risk assessment [7, 8]. Of particular relevance is the exceptional affinity of π-conjugated polymers like polystyrene (PS) for aromatic compounds via π-π stacking interactions, a mechanism that extends beyond simple hydrophobic partitioning [9, 10]. Multiple studies have demonstrated that PS exhibits substantially higher sorption capacity for aromatic contaminants than non-conjugated polymers (e.g., polyethylene, PE), owing to the matching aromatic ring structures of PS and target compounds [7, 11]. This molecular recognition capability, rooted in benzene ring moieties, distinguishes the environmental behavior of π-conjugated plastics from their non-conjugated counterparts [8, 11–13]. The significance of such π-conjugated interfaces is further underscored by recent advances across materials and environmental science [14, 15]. For example, spectroscopic evidence (e.g., FTIR peak shifts) has directly confirmed the role of π-π interactions in structuring hybrid organic-inorganic materials involving polystyrene [16]. Concurrently, engineered carbonaceous adsorbents derived from plastic waste have demonstrated efficient removal of polystyrene microplastics, with mechanisms explicitly attributed to π-π interactions and hydrogen bonding, supported by density functional theory calculations [17]. These lines of evidence collectively affirm that π-conjugated surfaces engage in specific, measurable interactions that govern pollutant fate and material properties. Despite this established understanding, the potential role of these intrinsic chemical interfacial properties in actively regulating microbial signaling and subsequently amplifying ecological risk has been largely overlooked [18].

The signaling molecule indole has emerged as a key regulator of microbial stress responses and horizontal gene transfer in environmental systems [19–21]. Produced by diverse bacteria as a tryptophan metabolite, indole functions as an interspecies signal that upregulates efflux pumps, activates SOS response pathways, and enhances bacterial tolerance to antibiotics [22–24]. Critically, the environmental concentration of indole is typically low and diffuse, limiting its ecological impact under natural conditions [25]. This limitation, however, could be overcome by anthropogenic materials capable of selective adsorption. Indeed, chemical signaling molecules like indole are recognized as direct modulators of bacterial stress and gene transfer [26, 27]. Despite its well-documented regulatory functions, the role of indole in mediating cross-kingdom interactions—particularly between fungi and bacteria—in the context of ARG dissemination remains poorly understood.

While the role of soil dissolved organic matter (DOM) in mediating pollutant interactions is recognized, the potential for specific chemical signaling at microplastic interfaces remains largely overlooked [6, 28]. The adsorption of DOM onto MPs modifies its composition and reactivity, which in turn influences contaminant bioavailability [6, 29]. Three-dimensional excitation-emission matrix (3D-EEM) coupled with PARAFAC modeling provides a powerful tool for probing these subtle interfacial changes at the molecular level [30, 31]. Concurrently, microbial communities assemble into intricate interaction networks that govern both the biodegradation of MPs and the dissemination of ARGs [32–34]. The formation of biofilms on MP surfaces increases bacterial cell-to-cell proximity, prolonging conjugation events and enhancing horizontal gene transfer [18]. Key genera, such as *Pseudomonas,* are known to degrade MPs through oxidative cleavage and hydrolysis, and their metabolic byproducts can profoundly alter the DOM pool [35]. This positions the microbiota as dual-function agents: active participants whose functions are co-regulated by chemically enriched signaling molecules.

Despite its ubiquity and known regulatory functions [19, 20, 36], the role of indole in mediating the nexus between the specific chemistry of anthropogenic pollutants and ARG dissemination remains poorly understood. We therefore hypothesized that the surface chemistry of π-conjugated anthropogenic pollutants serves as a "chemical interface hazard amplifier," proactively escalating environmental risk by concentrating key microbial signals and thereby programming risk-prone ecological networks. To test this, we employed π-conjugated (polystyrene, PS) and non-conjugated (polyethylene, PE) microplastics in a soil microcosm experiment. Our work uniquely integrates molecular dynamics simulations, multi-omics (3D-EEM, high-throughput sequencing), and advanced statistical modeling (co-occurrence networks, structural equation modeling) to quantify the causal pathways and resultant hazard of ARG dissemination. This approach transcends the traditional plastisphere paradigm by revealing a chemically driven, signal-dependent mechanism of resistance spread, establishing "**chemical interfacial-driven network engineering**" as a fundamental framework for environmental resistome evolution.

2. Materials and methods

2.1. Experimental design

Surface soil (0–10 cm depth) was collected from an agricultural field in Yixing, Wuxi City, Jiangsu Province, China. Soil was air-dried, homogenized, and sieved (2 mm mesh) to remove stones and plant residues. The soil properties were as follows: loam texture, pH 7.31, organic matter 6.18 g kg^{-1}, and particle composition of 46.8 % sand (2–0.02 mm), 38.3 % silt (0.02–0.002 mm), and 14.9 % clay (<0.002 mm). The polymer types were selected to represent the archetypal contrast between a non-conjugated alkane chain (PE) and a π-conjugated aromatic system (PS). Before the experiment, the microplastics were characterized for surface properties. Specific surface area, pore volume, and pore size distribution of the microplastics were determined via N_2 physisorption at 77 K using a surface area and porosity analyzer (Micromeritics ASAP 2460). As shown in Table 1, PS and PE exhibited similar Brunauer-Emmett-Teller (BET) surface areas (8.16 vs. 7.74 m^2/g) and total pore volumes (0.01754 vs. 0.01758 cm^3/g), but differed dramatically in surface charge and pore structure distribution. PS had a strong positive surface charge (+50.7 mV), whereas PE was negatively charged (-35.6 mV). PE possessed a higher micropore area (19.76 vs. 4.08 m^2/g) and micropore volume (0.0073 vs. 0.0016 cm^3/g) than PS, indicating distinct pore size distributions. (Table 2)

Table 1
Surface properties and Zeta potential of microplastics of PE and PS.

Properties	PE	PS
BET surface area ($m^2\ g^{-1}$)	7.74	8.16
t-Plot micropore area ($m^2\ g^{-1}$)	19.76	4.08
Langmuir surface area ($m^2\ g^{-1}$)	4.79	10.93
total pore volume ($cm^3\ g^{-1}$)	0.01758	0.01754
t-Plot micropore volume ($cm^3\ g^{-1}$)	0.0073	0.0016
Zeta potentials	-35.6	50.7

Table 2
Spectral information and description of the fluorescent components in soil. Two components were compared with previous studies using the OpenFluor database.

Component	Max. wavelength (Ex/Em, nm)	ex/em ranges (nm)	Description	Previous studies
C1	230/410	220–300/ 330–490	terrestrial humic substance-like	C1 [37]
			Terrestrial humic acid/ fulvic acid	C1 [38]
C2	300/390	280–330/ 320–480	Microbial activities/ Marine humic-like	C2 [39]

A controlled microcosm experiment included 15 treatments (each in triplicate): a blank control (CK); Indole-only treatments: 15 mg kg^{-1} soil (Y15) and 150 mg kg^{-1} soil (Y150); PE (10 μm spherical MPs) treatments: alone (0.2 %: PE0_2; 1 %: PE1) and combined with indole (Y15PE0_2, Y15PE1, Y150PE0_2, Y150PE1); and PS (10 μm spherical MPs) treatments: alone (0.2 %: PS0_2; 1 %: PS1) and combined with indole (Y15PS0_2, Y15PS1, Y150PS0_2, Y150PS1). The 10 μm particle size was selected based on environmental relevance, as recent studies have shown that microplastics in agricultural soils predominantly fall within the 10–500 μm size range [40]. The addition levels of 0.2 % and 1 % (w/w) were chosen to represent environmentally relevant concentrations, as field studies have reported microplastic concentrations ranging from 0.01 % to 1 % in agricultural soils [41]. In this study, two indole concentrations, 15 mg kg^{-1} and 150 mg kg^{-1}, were selected based on the actual environmental conditions. Existing research indicates that the concentration of 15 mg/kg can represent the indole background level commonly found in the environment [21]. In specific locations such as human and animal feces, intense biological metabolism leads to the accumulation of high indole concentrations [25, 42]. The concentration of 150 mg kg^{-1} was set to simulate the "indole hotspots" in such areas. By setting these two concentrations, we comprehensively covered the concentration range of indole in the actual environment, ensuring that the experimental results are highly relevant to diverse soil environmental scenarios [21, 42]. All microcosms were incubated statically at 25 °C for 8 weeks at 40 % moisture (w/w), with soil moisture maintained by biweekly replenishment of sterile water.

2.2. Three-dimensional excitation-emission matrix (3D-EEM) analysis

DOM was extracted by shaking soil-water mixtures (1:10, w/v) at 160 rpm for 4 h and then filtered through a 0.45 μm membrane. Total carbon (TC) and organic carbon (TOC) were analyzed using a TOC-L CPN analyzer (Shimadzu, Japan). The detailed experimental information is presented in Text S1 [39,43,44].

2.3. qPCR assay of antibiotic resistance genes

Soil DNA extraction was performed by Shanghai Meiji Biomedical Technology Co., LTD. Total DNA was extracted using the E.Z.N.A.® Soil DNA Kit (Omega Bio-tek, Norcross, GA, USA.) according to the manufacturer's instructions. The absolute abundance of six target genes—sulfonamide resistance genes (*sul1*, *sul2*), β-lactam resistance genes (*blaTEM*, *blaCTX-M*), and the class 1 integron-integrase gene (*intI1*) was quantified. Primer details are provided in Table S1 [45, 46]. The detailed experimental information of qPCR analysis is presented in Text S2.

2.4. High-throughput sequencing and analysis

High-throughput sequencing and data analysis were performed by Shanghai Meiji Biomedical Technology Co., Ltd. The V3-V4 region of the bacterial 16S rRNA gene and the ITS1 region of fungi were amplified and sequenced. For bacteria, the barcoded universal primers 338 F/806 R were used. For fungi, the ITS1F/ITS2 primer set was employed [47]. The data have been deposited in the National Microbial Sciences Data Center (NMDC) under accession number NMDC40060427. The detailed bioinformatic processing is shown in Text S3.

2.5. Molecular simulation and experimental validation of microplastic-indole interactions

Molecular dynamics simulations were conducted using the Forcite module within Materials Studio 2023 (Accelrys, San Diego, CA). PS and PE models were constructed as polymer chains, each containing 15 repeat units (PS: styrene units; PE: ethylene units). Composite models were constructed, each comprising one polymer chain and five indole molecules. Simulations were performed in vacuo to elucidate the intrinsic polymer-indole interaction energies; the qualitative trend in the relative difference between PS and PE is expected to be consistent regardless of solvent model. The convergence criteria for the geometry optimization and energy calculations were set as follows: (a) Forcefield: COMPASSIII; (b) Temperature: 298 K; (c) Electrostatic summation: Ewald (Accuracy 10^{-5} kcal/mol 10^{-5} kcal/mol); Van der Waals summation: Atom-based (Cutoff distance: 12.5 Å); (d) Geometry optimization settings: Segment lookahead: 1, maximum iterations: 1000.

Interaction energy was calculated as :

$$E_{int} = E_{total} - (E_{polymer} + E_{indole})$$

Where E_{total} represents the total energy of the system, and $E_{polymer}$ and E_{indole} represent the energies of the polymer and indole molecules, respectively. A lower (more negative) E_{int} indicates stronger binding affinity. An energy decomposition analysis was performed to partition the total interaction energy into its electrostatic and van der Waals components. All simulations were performed in triplicate to ensure reproducibility.

For experimental validation of the interfacial interaction, batch adsorption experiments followed by Fourier-transform infrared spectroscopy (FTIR) analysis were conducted. Detailed procedures are provided in Text S4.

2.6. Statistical analysis

Statistical analyses were conducted using the Auspicious Cloud platform (https://cloud.majorbio.com) to ensure standardization and reliability. Distance-based redundancy analysis (db-RDA) was used to examine the association between soil microbial community structure and physicochemical factors (e.g., organic matter, microplastic types, and ARG abundance). Co-occurrence networks of bacteria and fungi with environmental factors, ARGs, and *intI1* in PE/PS-contaminated soil were constructed based on Spearman correlation ($p < 0.01$, $|r| \geq 0.6$). PICRUSt2 (v2.2.0) and FAPROTAX (v1.2.1) were used to predict changes in the metabolic functional profiles of soil microbial communities. To quantify the causal pathways linking polymer chemistry, interfacial signal amplification, and consequent ecological risk, we constructed a structural equation model (SEM) that explicitly incorporated key environmental intermediates. Exogenous variables included polymer type (PS/PE) and indole concentration. Endogenous variables represented critical processes: DOM transformation (represented by its two major fluorescent components, C1 and C2), microbial community restructuring (bacterial and fungal community composition), relative abundance of keystone taxa (e.g., *Pseudomonas*, *Pseudeurotium*), and the target response variable (total ARG abundance). Model fit was evaluated using the comparative fit index (CFI), root mean square error of approximation (RMSEA), and chi-square statistic. The model was refined iteratively to achieve an optimal fit (CFI > 0.9, RMSEA < 0.08)

[48]. Specifically, Mantel tests were used to assess correlations between factors. Significant factors were transformed into matrices based on Bray-Curtis's dissimilarity and used as input for SEM construction in SPSS Amos 26.

3. Results

3.1. PS-indole synergy amplifies microbial activity and alters risk-associated DOM profiles

PARAFAC modeling identified two humic-like components: C1 and C2 (Fig. 1a; Table 1). Component abundances were quantified via F_{max} outputs from DOMFluor (Fig. 1b). Spectral characterization revealed that C1 (Ex/Em: 220–300 nm / 330–490 nm) showed strong fluorescence in the UVC range characteristic of humic-like substances, consistent with terrestrial humic/fulvic acids reported by Bianchi et al. [37] and Shakil et al. [38]; C2 (Ex/Em: 280–330 nm / 320–420 nm) exhibited UVB excitation characteristics associated with macromolecular hydrophobicity [39], indicating a microbial origin.

Co-exposure to MPs and indole significantly reduced both TC and TOC levels (Fig. S1a, b). Soil TOC content differed significantly among treatments. Relative to the CK, TOC was significantly reduced in both the PS-only and PE-only treatments ($p < 0.05$). In the combined treatments, the TOC content of PS-indole combinations (e.g., Y15PS0_2, Y150PS1) showed no significant difference from that of the PS-only treatment; whereas the TOC content of PE-indole combinations (e.g., Y15PE0_2, Y150PE1) exhibited no significant difference from that of the PE-only treatment. Most notably, TOC in Y150PS0_2 soils (22.19 mg/kg) decreased by 13.5 % compared to the PS0_2 (25.66 mg/kg), indicating enhanced microbial mineralization activity linked to the PS-indole synergy. Importantly, these treatments induced a specific reconfiguration of DOM fluorescence signatures (Fig. 1b): PE/PS generally increased the C1 component (terrestrial fulvic acid-like), but the Y150PE0_2 treatment counteracted this effect. In contrast, most MPs' treatments reduced the C2 component (microbially derived humic-like), with the exception of Y150PE1. Indole alone exerted minimal influence on either element.

Quantitative assessment of humification processes (Fig. 1c) revealed that HIX increased across treatments, reaching a peak of 4.9 in Y150PE0.2 soils, confirming the stabilization of DOM. The FI remained essentially unchanged (FI < 1.9, indicating persistent terrestrial DOM signatures), but increased in the Y15, Y150PE0_2, Y150PE1, and Y15PS0_2 treatments.

3.2. Polymer chemistry dictates microbial community restructuring

Treatment-specific shifts in the relative abundance of the top 20 bacterial and fungal genera are shown in Fig. 2. Specifically, the PS amendments selectively suppressed the abundance of *Arthrobacter*. At the same time, co-exposure with high-dose Indole (Y150PS) significantly enriched *Bacillus* (Fig. 2a). For fungi, low-dose indole enhanced PE-driven enrichment of *Engyodontium*, whereas high-dose indole inhibited its proliferation. PS and PS-indole treatments consistently increased the beneficial fungus *Talaromyces* (Fig. 2b).

LEfSe analysis revealed taxon-specific biomarkers (Fig. 2c, d). For bacteria, PS treatment selectively enriched *Actinocorallia* and *Rhodococcus*, while PE uniquely promoted *Polycyclovorans* (Fig. 2c). The application of indole consistently increased the abundance of *Cupriavidus*. Notably, the Y150PS0_2 treatment exhibited the highest LDA scores for *Pseudomonas* and *Bacillus* (Fig. 2c), and their abundances were

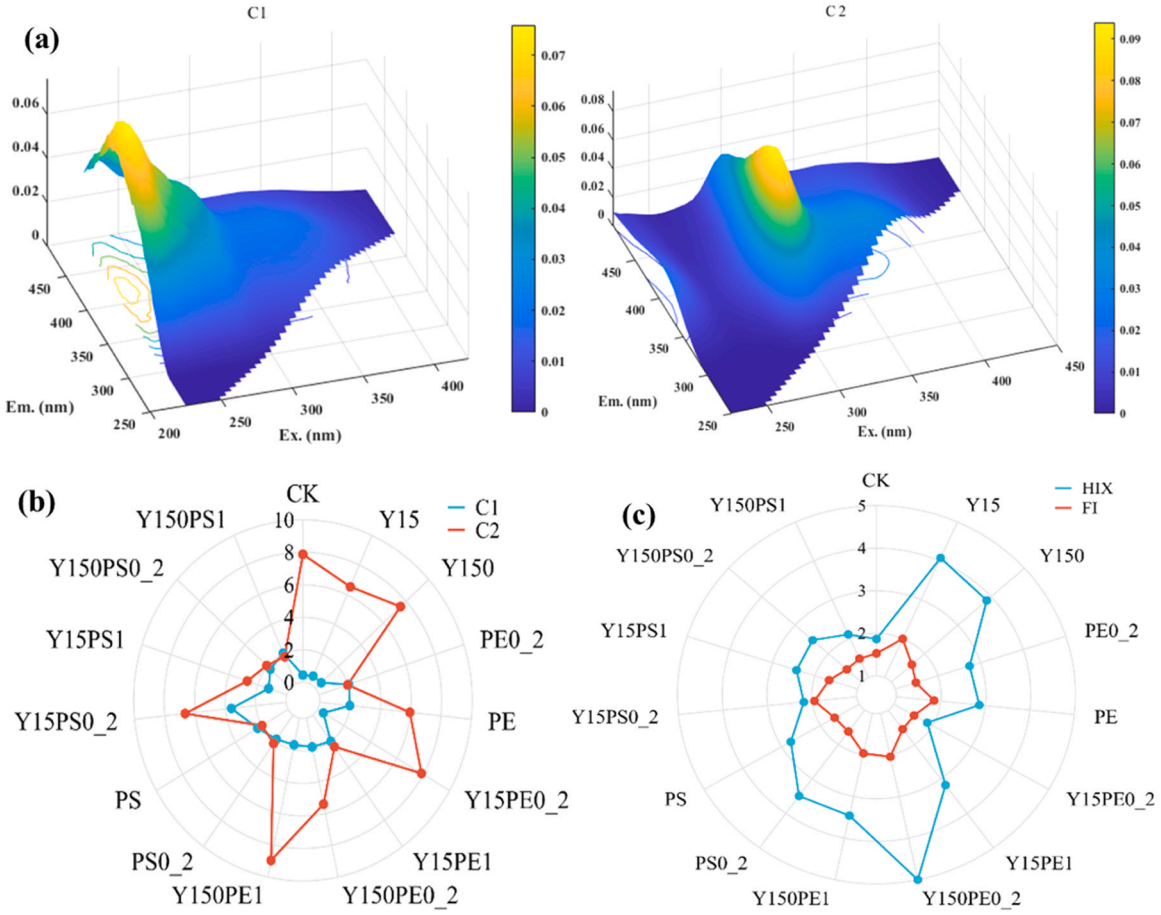

Fig. 1. Effects of indole and MPs on soil DOM: (a) PARAFAC-derived EEM contours; (b) Component abundance; (c) HIX/FI indices.

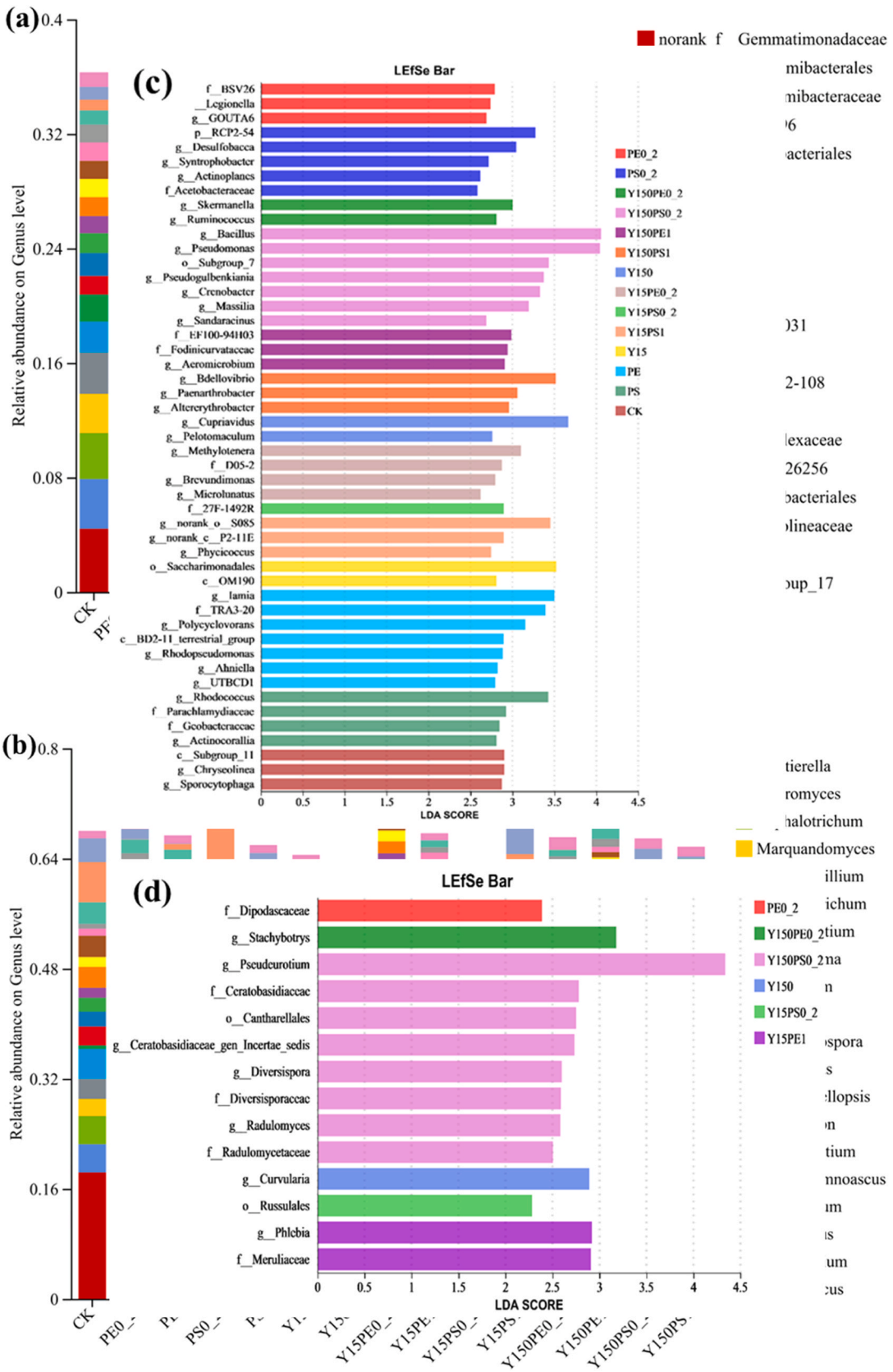

Fig. 2. Microbial community responses to the treatment of indole and MPs: Top 20 bacterial (a) and fungal (b) genera; LEfSe analysis of bacteria (c) and fungi (d).

confirmed to be significantly elevated ($p < 0.05$) relative to CK (Fig. S2). Furthermore, the relative abundances of *Pseudomonas* and *Bacillus* in this treatment were significantly higher than in all other groups except Y150PS1. For fungi, Y150PS0_2 uniquely enriched eight fungal genera,

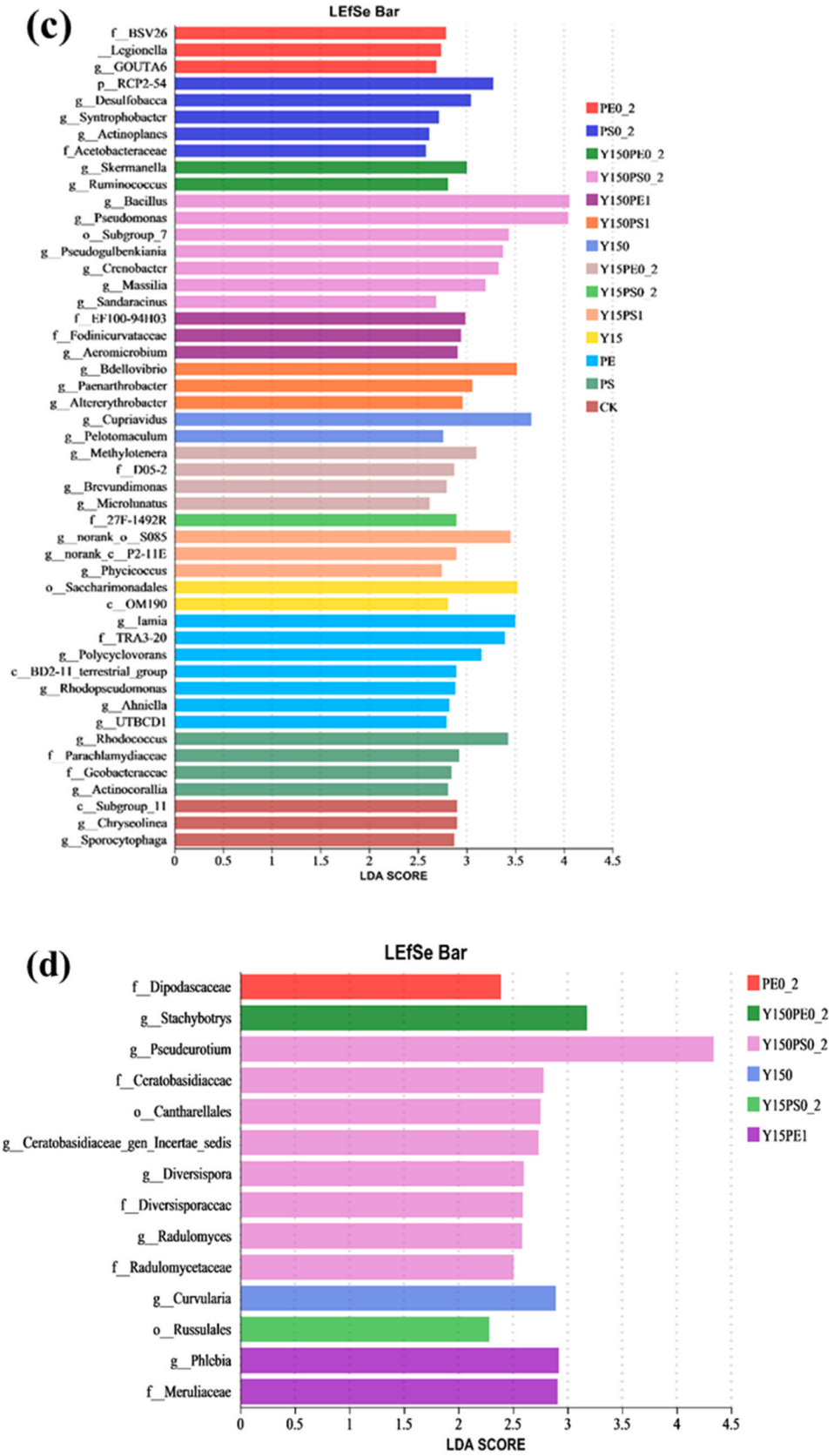

Fig. 2. (*continued*).

most notably *Pseudeurotium* (highest LDA > 4.3). PE0_2, Y150PE0_2, and Y150 were characterized by *Dipodascaceae*, *Stachybotrys*, and *Curvularia*, respectively.

Functional predictions (PICRUSt2) indicated treatment-driven metabolic reprogramming. Y150PS0_2 marginally increased *Pseudomonas aeruginosa* biofilm formation (+19 %, $p > 0.05$; Fig. S3a) but

significantly enhanced β-lactam resistance ($p < 0.05$; Fig. S3b). Complementary FAPROTAX analysis revealed that PS treatments profoundly stimulated hydrocarbon degradation functions: aliphatic non-methane hydrocarbon degradation increased 13.8-fold, aromatic hydrocarbon degradation increased 11.2-fold, and total hydrocarbon degradation increased 4.2-fold compared to CK (Fig. S4). This functional reprogramming demonstrates that PS-indole synergy selects for a specialized microbial phenotype. The phenotype is adept at exploiting pollutant-enriched niches and aligning catabolic potential with ecological opportunity.

3.3. Chemical interfacial-dependent amplification of antibiotic resistance gene hazard

While both PE and PS alone modestly increased the abundance of the mobile genetic element *intI1*, co-exposure with high-dose Indole (Y150) resulted in dramatic, polymer-dependent amplification: a 2.9-fold increase in *intI1* occurred in the Y150PS0_2 treatment, the highest among all experimental conditions (Fig. 3a). Crucially, the abundance of *sul2*—a sulfonamide resistance gene prevalent in clinical isolates—exhibited a stark, polymer-dependent response (Fig. 3b). While PS alone had a marginal effect and PE was ineffective, combining PS with high-dose indole (Y150PS0_2) triggered a 2.1-fold increase in *sul2* abundance ($p < 0.05$). This stark contrast provides direct evidence that the enhancement of clinically relevant ARGs is contingent upon the specific chemical interaction between PS and indole, rather than the generic physical presence of a polymer. Similar polymer-specific induction was observed for β-lactam resistance genes (*blaTEM*, *blaCTX-M*), where high-dose indole was the primary driver of this effect. Still, the magnitude of induction was always greater in the presence of PS compared to PE (Fig. 3c).

3.4. Microbial community assembly is driven by chemical interfaces and co-occurs with ARG hotspots

db-RDA analysis revealed that environmental factors collectively explained 8.19 % of the total variation in the bacterial community, with distinct polymer-specific clustering: the PE-treated (blue ellipse) and PS-treated (green ellipse) groups formed separate clusters (Fig. 4a), demonstrating concentration-dependent restructuring influenced by the chemistry of MPs. Treatment factors—PE (21.9 %), PS (33.8 %), and Indole (24.8 %)—emerged as primary drivers of bacterial reorganization ($p < 0.05$; Table S2), with ARGs predominantly associated with high-indole PS co-exposure groups. Notably, *sul2* exerted a significant influence on bacterial community structure ($r^2 = 26.5$ %, $p < 0.01$).

For fungal communities, environmental factors explained 8.04 % of the total variation while maintaining clear chemical-specific separation (PE vs. PS; Fig. 4b). DOM components C1 ($r^2 = 0.269$) and C2 ($r^2 = 0.428$) were key determinants of fungal assemblage shifts (Table S3). Critically, *sul2* showed the strongest association with fungal community dynamics ($r^2 = 27.6$ %, $p < 0.01$), indicating that fungi may act as potential vectors for *sul2* transmission.

3.5. A keystone fungus architects a cross-kingdom network for ARG transmission

Co-occurrence network analysis revealed a stark contrast in microbial interaction architecture between PE- and PS-contaminated soils (Fig. 5). In PE systems, indole acted as a relatively diffuse signal, correlating with several bacterial genera, but no clear cross-kingdom hubs emerged (Fig. 5a). In stark contrast, PS contamination fostered a highly structured, interconnected network centered around the keystone fungus *Pseudeurotium* (Fig. 5b). This taxon exhibited unparalleled connectivity, forming statistically robust positive correlations ($r > 0.6$, $p < 0.01$) not only with the signal molecule indole, but also with the primary bacterial degraders *Pseudomonas* ($r = 0.61$), *Cupriavidus* ($r = 0.67$), and *Bacillus* ($r = 0.74$). Crucially, *Pseudeurotium* simultaneously correlated with the dissemination of multiple ARGs (*intI1*, *sul2*, *blaCTX-M*, *blaTEM*), acting as a central conduit for resistance gene spread. Topological analysis confirmed *Pseudeurotium*'s central role: it possessed the highest betweenness centrality (0.41) and radiality (0.90) among all detected taxa, making it the most critical bridge connecting the amplified indole signal to bacterial degraders and ARG dissemination. These network analyses strongly suggest a departure from the conventional, bacteria-centric model and point to a role for fungi, such as *Pseudeurotium*, as potential active agents in ARG transmission networks (Table S4).

3.6. Molecular selectivity of π-conjugated surfaces creates indole hotspots

We first quantified the fundamental chemical interaction underpinning our hypothesis. Molecular dynamics simulations revealed that PS-indole binding energy (−128.56 kcal/mol) was 2.42-fold stronger than PE-indole (−53.21 kcal/mol) (Fig. 6a). Energy decomposition analysis showed that PS binding was driven by van der Waals forces (−83.80 kcal/mol, 76.1 %) and electrostatic contributions (−16.72 kcal/mol, 15.2 %), characteristic of π–π stacking interactions. In contrast, PE-indole binding relied solely on van der Waals forces (Fig. 6b). Although the BET surface areas of PS and PE were similar (Table 1), their surface chemistry dictated profoundly different affinities for indole. This molecular selectivity explains why PS, but not PE, enhanced ARG dissemination when combined with indole. The PS-indole complex adopted a stable T-shaped configuration (inter-ring distance: 5.1 Å), as visualized by electron density and electrostatic potential maps (Fig. 6b inset). In contrast, the PE-indole interaction lacks any specific recognition motif, relying solely on weak, non-directional van der Waals forces.

FTIR spectroscopy delivered conclusive molecular-scale evidence for the specific, multi-modal interactions that define the PS-indole interface (Fig. 6c). The spectrum of the complex revealed a hierarchical set of diagnostic changes, far surpassing a simple additive profile. First and foremost, the aromatic C–H out-of-plane bending vibration of PS exhibited a pronounced redshift from 713 to 693 cm^{-1} . This shift is a direct spectroscopic signature of the perturbed π-electron cloud in the PS benzene ring, providing definitive evidence for core π-π stacking interactions. In addition, the chemical immobilization of indole was confirmed by the emergence of two new peaks at 1600 and 1640 cm^{-1} —characteristic aromatic stretching vibrations of indole that are absent in pure PS. Concurrently, a subtle blue shift of another indole peak (from 742 to 746 cm^{-1}) alongside the marked enhancement of peaks at 1450 and 1491 cm^{-1} , indicates both electronic perturbation and intense local enrichment of indole at the interface. Third, the indole N–H stretching band underwent a substantial broadening and redshift from 3396 cm^{-1} to the 3100–3700 cm^{-1} range, a classic indicator of auxiliary N-H···π hydrogen bonding that cooperatively stabilizes the adsorption complex. In stark contrast, none of these specific spectral alterations were observed for the PE-indole system, which displayed only features of non-specific physisorption.

This direct evidence for multifaceted molecular recognition provides the fundamental mechanistic explanation for the decisive functional disparity: PS adsorbed 1.71-fold more indole than PE (1.52 vs. 0.89 mg g^{-1}; Fig. S5). Critically, this superior chemical affinity of PS was established despite PE's structural advantages, including greater micropore volume and a mesopore-favored architecture (Table 1, Fig. S6). Therefore, these results conclusively demonstrate that the formation of potent interfacial signaling hotspots is governed not by physical texture, but by the specific chemical interactions (π-π stacking and cooperative hydrogen bonding) inherent to π-conjugated surfaces. This chemically driven, selective amplification of a microbial signal constitutes the essential molecular-scale trigger for the subsequent ecological cascade.

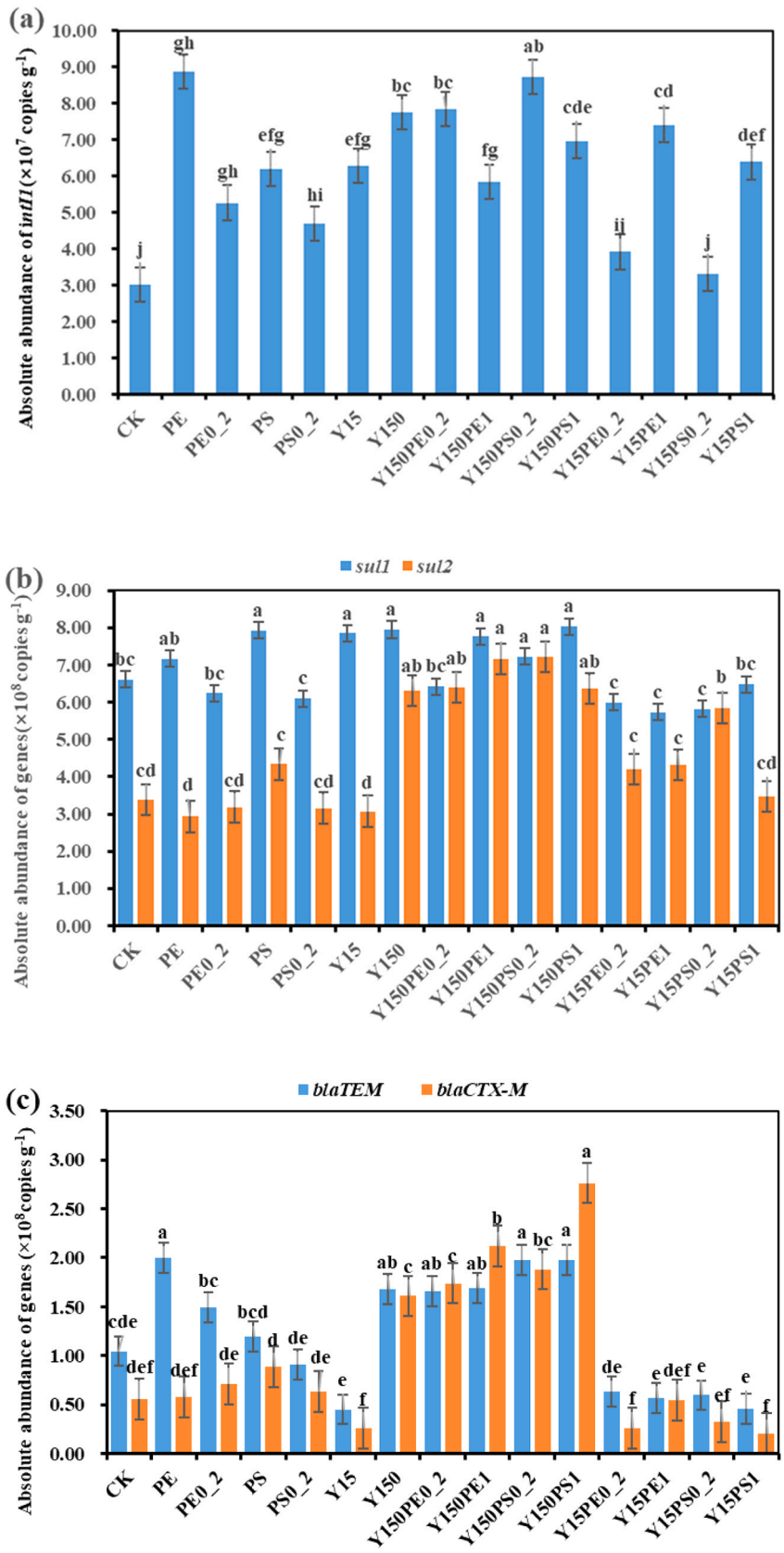

Fig. 3. The effects of PE, PS, and indole on the *intl1*and antibiotic resistance genes in soil. (a) *intI1*; (b) *sul1* and *sul2*; (c) *blaTEM* and *blaCTX-M*.

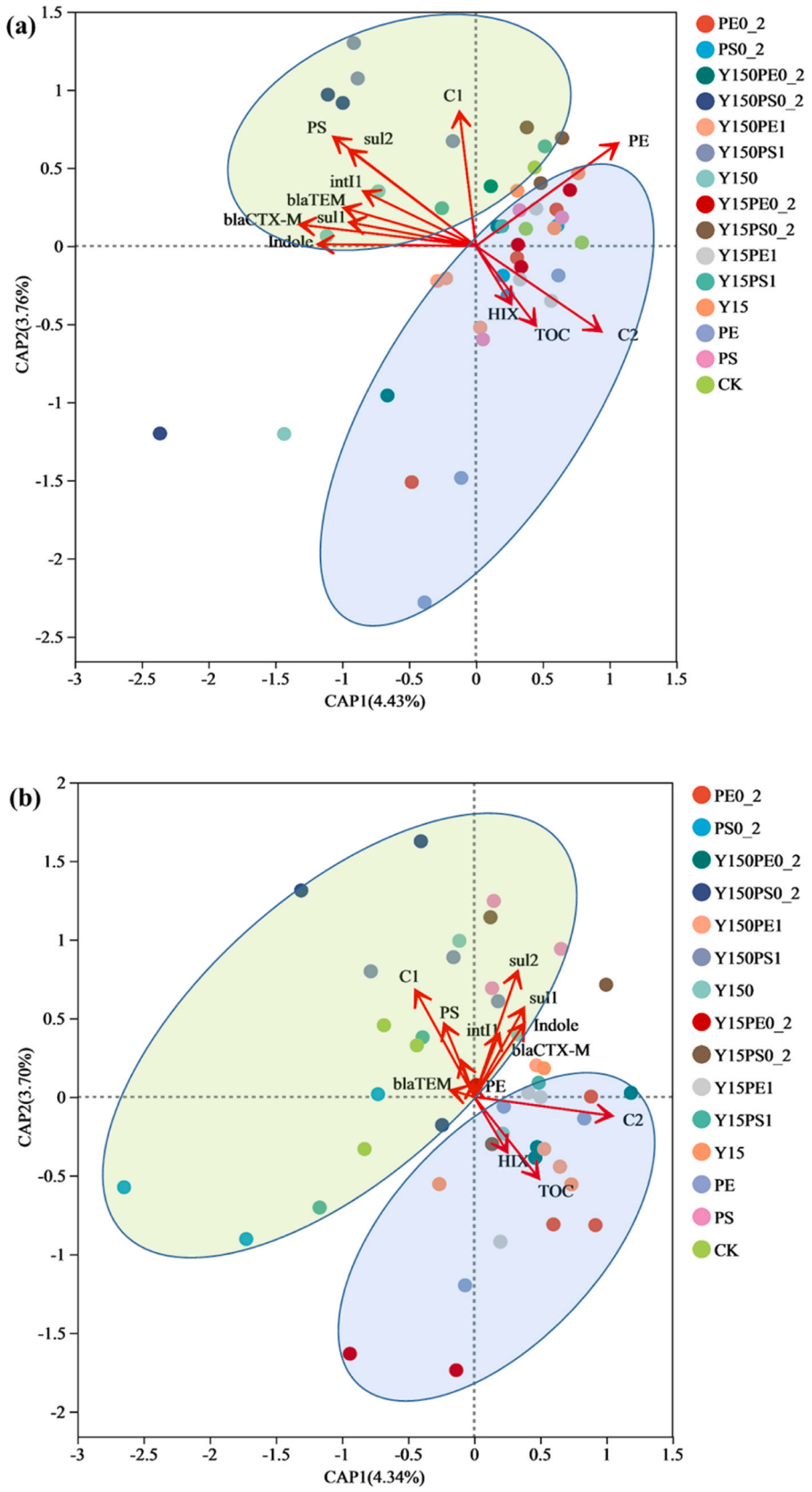

Fig. 4. Effects of indole and PE/PS on soil bacterial (a) and fungal (b) communities based on db-RDA at genus level.

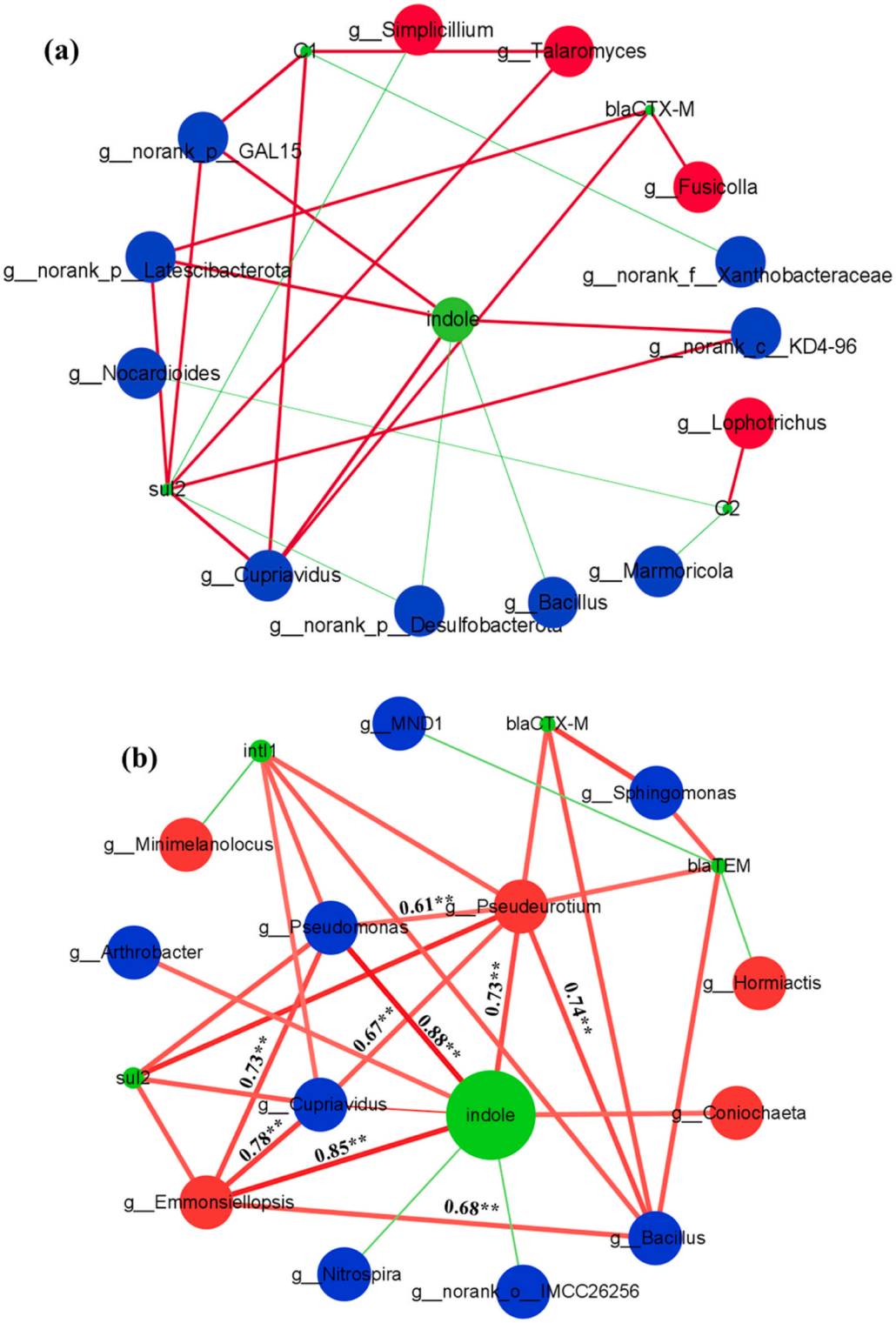

Fig. 5. Cross-kingdom co-occurrence networks linking microbial taxa with environmental variables and antibiotic resistance genes in PE (a) and PS (b) contaminated soils. The size of species nodes represents abundance, with red nodes representing bacteria and green nodes representing fungi. The thickness of the lines represents the strength of the correlation; red and green lines represent positive and negative correlations, respectively, with more lines indicating closer connections between nodes.

3.7. Structural equation modeling quantifies causal drivers

This quantitative disparity in adsorption energy is directly reflected in a hierarchy of biological causality. The amplified indole signal, rather than the polymer, is the dominant driver of ARGs. To dissect biological causality, we employed structural equation modeling (CFI = 0.90, RMSEA = 0.065). The model (Fig. 7; full results in Table S5) not only quantified the dominant role of the amplified indole signal ($\beta = 0.47$, $p < 0.001$) but also revealed the significant mediating roles of specific environmental variables. Notably, the DOM component C2 exhibited a

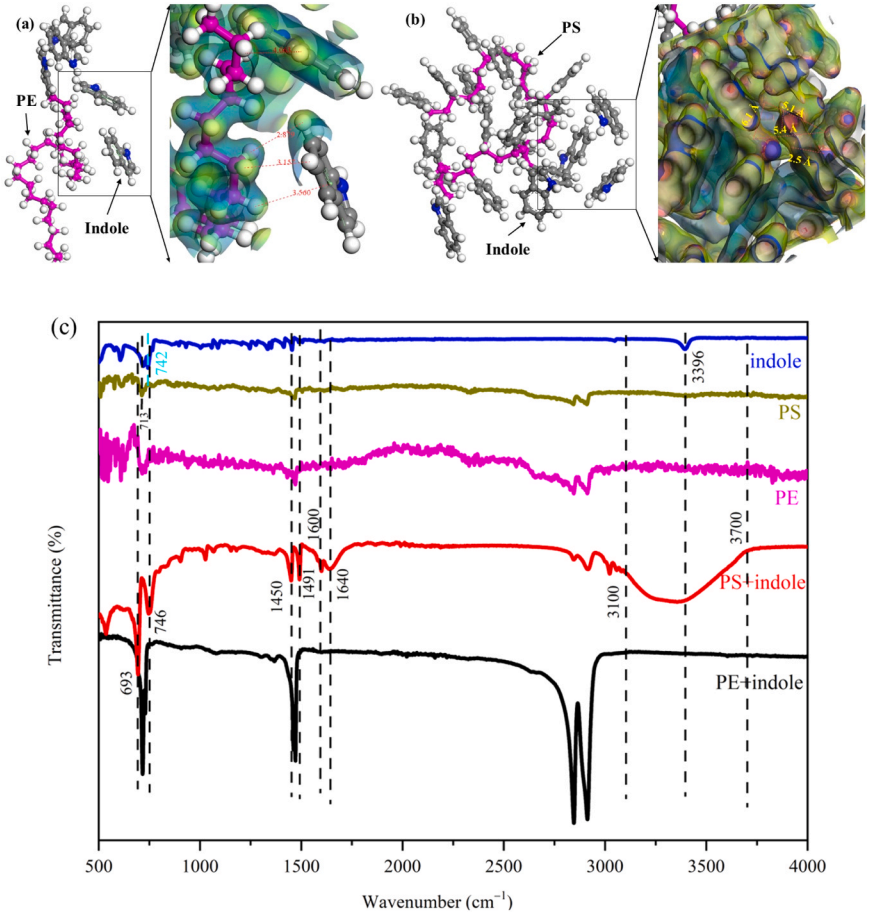

Fig. 6. Molecular simulation of optimized structures of PE-indole and PS-indole systems. (a) The conformation of the PE-indole system (interaction energy: −53.21 kcal/mol); (b) The most stable conformation of the PS-indole system (interaction energy: −128.56 kcal/mol), local magnification showing a T-shaped typical π-π stack (d = 5.1 Å). The magnified region shows the electron cloud density and electrostatic potential map; the distance is the H atom spacing or centroid distance; (c) FTIR spectra of indole before and after complexation with microplastics PE and PS.

standardized total effect of 0.008 on ARGs, indicating that microbially derived humic-like substances, whose composition was altered by treatments (Fig. 1), contributed to the risk pathway. The fungal community, particularly through the keystone taxon *Pseudeurotium* (direct effect $\beta = 0.07$, $p < 0.05$), acted as a critical biological conduit. In contrast, the direct effects of the bulk bacterial community composition and the terrestrial humic-like component (C1) on ARGs were not significant in the final model, suggesting that risk amplification is channeled through more specific fungal and DOM signatures rather than broad community shifts or all DOM types. These findings definitively establish that the amplified indole signal, enabled by PS surface chemistry, is the primary driver of ARG dissemination, with the fungal-bacterial alliance acting as its essential conduit for transmission.

4. Discussion

4.1. Polymer-specific chemical interactions underpin selective signal amplification

Our results demonstrate that the amplification of ecological risk observed for PS microplastics in the presence of indole is fundamentally rooted in polymer-specific surface chemistry, rather than non-specific physical properties. This aligns with the established understanding that the sorption behavior of microplastics is governed by their molecular structure and interfacial properties [18, 49, 50]. Notably, although PS and PE possessed comparable BET surface areas and total pore volumes (Table 1), they differed dramatically in surface charge and pore-size distribution. The key distinction lies in the π-conjugated aromatic rings of PS, which confer a high, well-documented affinity for aromatic compounds via π-π stacking—a mechanism far less effective in non-conjugated polymers like PE [51, 52]. Consistent with this principle, our molecular dynamics simulations revealed that the PS-indole binding energy (−128.56 kcal/mol) was 2.42-fold stronger than that of PE-indole (Fig. 6a, b), a difference driven primarily by specific π-π stacking in PS, as opposed to non-specific van der Waals forces in PE. This pronounced difference in binding energy and mechanism occurred despite PE having a larger micropore area and volume, reinforcing that textural properties alone cannot explain the selective signal enrichment. This computational finding was experimentally validated: FTIR spectroscopy confirmed characteristic spectral shifts indicative of π-π interactions in PS–indole complexes, which were absent in PE–indole systems (Fig. 6c), and PS exhibited a 1.71-fold higher adsorption capacity for indole (Fig. S5). Consequently, the π-conjugated surface of PS acts as a selective “chemical antenna,” effectively concentrating the otherwise diffuse signal molecule indole into localized interfacial hotspots. This molecular-scale process, governed by chemical recognition rather than physical structure, provides the essential first link in the hazard-amplification chain, explaining the stark biological divergence between PS and PE observed in our microcosms.

4.2. From chemical hotspots to genetic triggers: The primacy of amplified signaling

The pivotal insight from our structural equation modeling is the

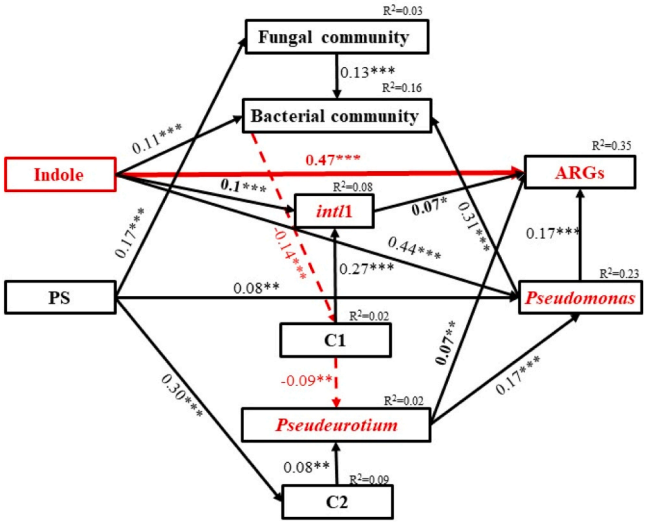

Fig. 7. The amplified indole signal is the dominant driver of ARG abundance. Structural equation model quantifying the direct and indirect effects of polymer type, indole, DOM (C1 and C2), microbial community (bacterial and fungal community composition), and keystone taxa (*Pseudomonas*, *Pseudeurotium*), on ARG abundance. The path coefficient for indole (β = 0.47) was 23.5-fold greater than that of the PS polymer. SEM model parameters: Chi-square = 145.385, Degrees of freedom = 28, CFI = 0.9, TLI = 0.84, RMSEA = 0.065 ($p < 0.001$).

quantitative dominance of the amplified indole signal as the direct driver of ARG dissemination (β = 0.47), with the PS polymer itself playing a significantly weaker, indirect role (β = 0.02) (Fig. 7). This finding challenges the paradigm that microplastics act primarily as physical vectors for ARGs [53, 54], and elevates the role of chemical signaling at the microplastic interface. Indole is a recognized interspecies and interkingdom signaling molecule that regulates microbial stress responses, including the upregulation of efflux pumps and the activation of the SOS response (RecA-LexA pathway) [55–57]. Critically, beyond its role in bacterial stress, indole concentrated at the PS interface likely acts as a potent mediator of bacterial-fungal interactions. As highlighted in recent syntheses, competition for resources, often mediated by chemical signals, is a primary driver structuring soil microbial communities [58]. The localized, high-concentration indole hotspot created by PS may thus not only hyperactivate bacterial SOS and horizontal gene transfer but also trigger a cascade of interference and exploitative competition between bacteria and fungi [59]. This competition can profoundly reshape community composition and metabolic networks, favoring alliances adept at exploiting the chemically enriched niche [60]. We therefore propose a plausible mechanistic pathway: indole hotspots created by PS generate a localized, high-concentration signal field that potently activates the bacterial SOS response and re-engineers cross-kingdom interactions within proximal microbial communities. This, in turn, hyperactivates the genetic machinery underlying horizontal gene transfer, leading to the observed surge in *intI1* (2.9-fold increase) and clinically relevant ARGs like *sul2* (2.1-fold increase) specifically in PS-indole co-exposure treatments (Fig. 3). This model reconciles the seemingly paradoxical co-occurrence of enhanced hydrocarbon degradation (Fig. S4) and ARG spread, as both can be viewed as facets of a generalized microbial stress and adaptation response triggered by the chemically amplified signal.

4.3. The potential role of Pseudeurotium as a network hub in signal-amplified niches

The central role of *Pseudeurotium* within the cross-kingdom network assembled under PS-indole co-exposure suggests a departure from conventional, bacteria-centric models of ARG transfer in plastispheres. Our network analysis positioned this fungus as a highly connected hub, correlating with both the enriched indole signal and the abundance of key ARGs (e.g., *sul2*, *intI1*). While this pattern alone does not confirm mechanistic involvement, it aligns meaningfully with a growing body of research demonstrating that fungal mycelial networks can actively shape the distribution of antibiotic resistance in soil environments [61].

Specifically, Nazir et al. [62] provided direct experimental evidence that soil fungi serve as “novel ecological routes” for the enrichment and dissemination of ARGs. Their microcosm experiments showed that different fungal taxa selectively enriched distinct communities of antibiotic-resistant bacteria and facilitated their transport along hyphal networks, thereby spatially restructuring local ARG pools [63]. Importantly, they observed that fungal identity strongly influenced which ARGs and mobile genetic elements (e.g., *intI1*) were enriched, indicating that fungi are not passive substrates but active agents in resistome assembly [63]. This prior work supplies a plausible, empirically supported mechanism to interpret our correlative data: *Pseudeurotium*, enriched at the PS-indole interface, likely creates a selective mycosphere that recruits, retains, and potentially facilitates interaction among specific ARB hosts, thereby amplifying the local signal for ARG dissemination.

Our findings further contrast with the general model of plastisphere network assembly reported in broader MP research. Deng et al. [64] systematically demonstrated that microbial networks on diverse MPs exhibit lower complexity and stability than those in bulk soil and are primarily driven by bacterial interactions, with fungi playing a comparatively minor role. The PS-indole interface, rich in a hydrophobic aromatic signal, may selectively favor fungi such as *Pseudeurotium*—taxa often more competitive in utilizing hydrophobic compounds or niches [65]. This divergence underscores a key insight: the specific chemical interface of π-conjugated PS—through its capacity to concentrate signaling molecules like indole—can override generic plastisphere assembly rules. Rather than producing a typical, bacteria-dominated biofilm, this chemically “engineered” interface selects for a cross-kingdom network architecture in which a fungus becomes a critical connector.

Integrating these perspectives, we propose that *Pseudeurotium* functions as an ecological integrator within the chemically amplified niche. Its role may be twofold: (i) acting as a physical scaffold that enhances bacterial connectivity and co-localization (as demonstrated in fungal-vector studies [61, 63], and (ii) sustaining a microenvironment where the concentrated indole signal (the primary driver in our SEM, β = 0.47) upregulates bacterial stress-response and horizontal gene-transfer pathways. Thus, while direct proof of fungal-mediated plasmid transfer in our specific system awaits further experimentation, collectively, the convergence of our network topology with established fungal ecological functions [61] and its divergence from typical plastisphere networks [63] strongly supports the interpretation that *Pseudeurotium* is a key biological component in the ARG dissemination pathway facilitated by PS-indole interfacial chemistry.

4.4. Toward a universal framework: chemical interfacial-driven network engineering

Synthesizing the experimental and modeling evidence, we propose a Chemical Interfacial-Driven Network Engineering (CIDNE) model that reframes the ecological impact of anthropogenic surfaces (Fig. 8) and redefines the paradigm for microplastic-driven resistome evolution, as systematically contrasted with the traditional view in Table 3. This model extends the prevailing plastisphere concept by introducing a decisive, chemistry-driven layer of regulation. While the classical plastisphere paradigm effectively describes the microplastic surface as a physical scaffold for biofilm formation and proximity-enhanced gene transfer [64, 66], it largely overlooks the active chemical agency of the polymer interface in structuring microbial interactions. CIDNE addresses this gap by establishing that the inherent chemical functionality

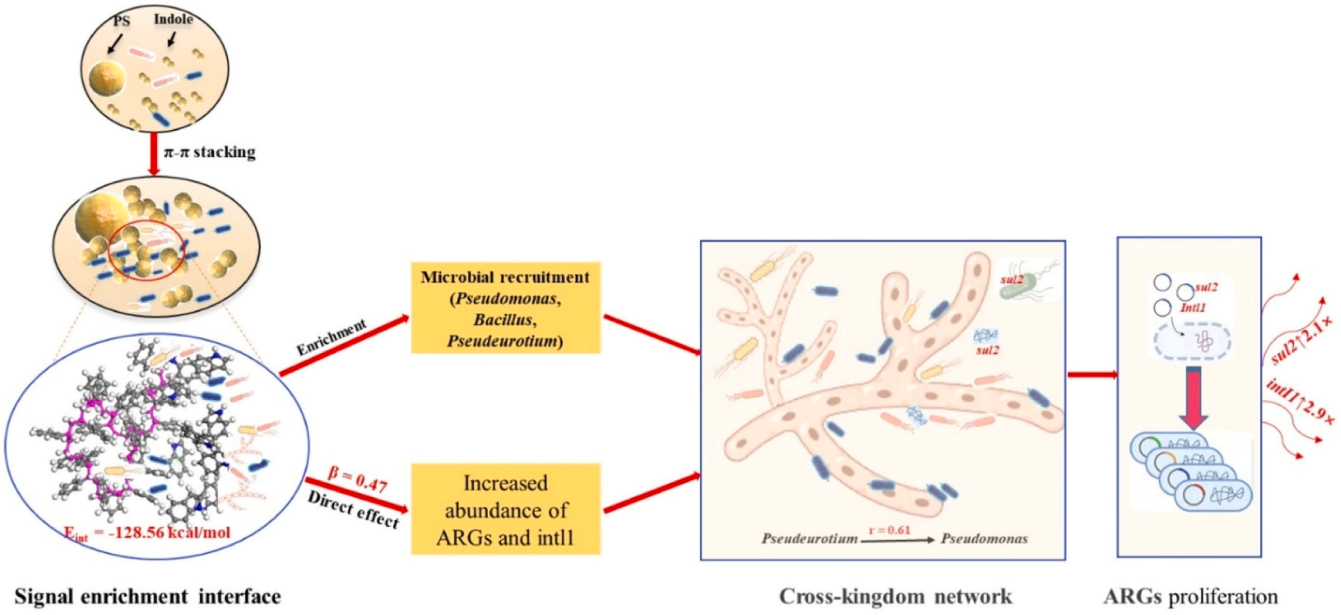

Fig. 8. Integrated "Chemical Interfacial-Driven Network Engineering model" of ARGs dissemination in PS-contaminated soils.

Table 3
Evolving the paradigm: from microplastics as passive carriers toward chemical interfacial-driven network engineers.

Cognitive dimension	Traditional paradigm	Central findings of this study	Evidence-informed perspective
Core driver	Physical presence and surface area of microplastics (inert substrate)	Amplified indole signal is the strongest direct correlate of ARG abundance (β = 0.47), vastly outweighing the polymer effect (β = 0.02; Fig. 7)	The chemically amplified signal at the interface, not the particle itself, emerges as the proximate risk driver
Surface recognition	Non-specific (hydrophobic) partitioning and adsorption capacity	PS exhibits specific π-π stacking with indole, adsorbing significantly more indole than PE despite PE's textural advantages (Fig. 6, S5; Table 1)	Molecular recognition via specific chemical interactions overrides the influence of generic physical texture
Microbial community assembly	Bacteria-dominated biofilm formation, promoting conjugation	PS-indole exposure engineers a cross-kingdom network centered on the keystone fungus *Pseudeurotium*, linking signal, degraders, and ARGs (Fig. 5b)	Interfaces can actively structure ecological networks, with fungi as critical hubs connecting signal to dissemination
Risk profile & origin	General increase in ARGs with microplastics	Polymer-specific synergy: Clinically relevant *sul2* increases significantly only with PS-high indole co-exposure (Fig. 3b) and strongly associates with fungal dynamics (Fig. 4b)	Risk is chemically contextual, arising from specific pollutant-signal synergies that reshape the resistome

of a polymer—specifically, its capacity for selective molecular recognition—can engineer ecological risk from the bottom up.

The core of the CIDNE framework is a hierarchy of causality, pivoting from physicochemical interaction to ecological consequence. It posits that the amplified chemical signaling of molecules like indole (path coefficient β = 0.47, Fig. 7)—enabled by specific interfacial interactions such as π-π stacking and electrostatic synergy (Fig. 6)—serves as the primary driver, rather than a passive byproduct. This signal amplification transcends generic hydrophobic adsorption and is governed by chemical properties like surface charge-polarity (Table 1) more than by physical texture. The concentrated signal, in turn, reprograms the local microbiome, selectively fostering a cross-kingdom network architecture. Crucially, this network shifts the focus from a bacteria-centric model to one where a keystone fungus (*Pseudeurotium*) acts as a critical hub, connecting the chemical hotspot to bacterial degraders and the dissemination of ARGs (Fig. 5b). Consequently, ARG transmission evolves from a process of passive conjugation to one of active, network-facilitated selection and propagation, as evidenced by the strong association between sul2 and the fungal community (Fig. 4b).

Collectively, the CIDNE framework provides a coherent, mechanism-based explanation for the stark functional divergence observed between PS and PE microplastics—a divergence that persisted despite their similar specific surface areas. This underscores that intrinsic chemical functionality, not general physical metrics, governs interfacial risk engineering. It thus catalyzes a paradigm shift: from viewing microplastics as passive physical vectors to recognizing their interfaces as active ecological engineers, capable of reprogramming microbial behavior and community networks through molecule-specific interactions. This refined perspective urges a future focus on the chemical-ecological pathways, rather than merely the mass, of anthropogenic pollutants in environmental risk assessment.

5. Conclusion

Based on our integrated experimental and modeling evidence, we demonstrate that π-conjugated PS microplastics, unlike their non-conjugated PE counterparts, function as active chemical amplifiers of antibiotic resistance in soil. This role is mediated not by generic physical properties but by a specific, sequential mechanism we term CIDNE. The CIDNE pathway initiates with molecular recognition: the π-conjugated surface of PS selectively concentrates the microbial signaling molecule indole via high-affinity interactions, primarily driven by π-π stacking with a significant electrostatic contribution, as elucidated by our molecular simulations and surface charge analysis. This creates localized interfacial hotspots, which in turn reprogram the soil habitat—evidenced by distinct dissolved organic matter transformation—and drive the assembly of a specialized, cross-kingdom microbial network architected around the keystone fungus

Pseudeurotium. Crucially, our structural equation modeling quantitatively establishes that the amplified indole signal itself is the paramount driver of ARG dissemination, with an effect vastly overshadowing that of the polymer particle.

These findings fundamentally redefine the ecological role of certain microplastics from inert physical vectors to active chemical engineers of microbial ecosystems. The CIDNE framework provides a mechanistic explanation for the divergent environmental risks posed by different polymers, emphasizing that chemical functionality at the interface—governed by specific molecular interactions—not merely abundance, dictates ecological impact. While derived from an agricultural soil system, the chemical principles underpinning CIDNE offer a new lens for assessing the interfacial activity of anthropogenic materials. Consequently, future strategies to mitigate the environmental spread of antibiotic resistance may need to target such specific chemical-ecological pathways, shifting the focus of risk assessment from pollutant mass to molecular interaction potential.

Environmental implication

This study establishes that π-conjugated microplastics, exemplified by polystyrene, function not as inert carriers but as proactive chemical amplifiers of environmental antibiotic resistance. Their capacity to selectively enrich signaling molecules (e.g., indole) and thereby engineer cross-kingdom microbial networks drives the enhanced dissemination of clinically relevant resistance genes. These findings coalesce into the **Chemical Interfacial-Driven Network Engineering (CIDNE)** framework, which points to a critical shift in risk assessment paradigms—from quantifying pollutant mass to deciphering interfacial molecular interactions. Ultimately, this mechanistic understanding redefines the source of risk for certain microplastics from their bulk presence to their specific interfacial chemical activity.

Environmental significance

This study reveals that the environmental risk of microplastics is governed by their specific interfacial chemistry, not merely their physical abundance. We demonstrate that π-conjugated microplastics like polystyrene act as “chemical hazard amplifiers” by selectively concentrating signaling molecules (e.g., indole) via specific π-π and electrostatic interactions, thereby reprogramming the local microbiome and forging cross-kingdom networks that potently facilitate the dissemination of clinically relevant antibiotic resistance genes (ARGs).

Most critically, our causal modeling identifies the amplified chemical signal, not the polymer particle itself, as the dominant driver of risk—a finding that challenges the prevailing paradigm of microplastics as passive physical vectors. This insight is synthesized into the Chemical Interfacial-Driven Network Engineering (CIDNE) framework, which describes how molecular-scale interactions at pollutant interfaces can cascade into ecosystem-level resistome amplification.

The CIDNE framework provides a novel, chemistry-aware lens for environmental risk assessment. It suggests that the hazard potential of anthropogenic materials co-depends on their inherent chemical functionality and the ecological context of signaling molecules. This principle urges a shift in risk mitigation from focusing solely on plastic mass to targeting the specific chemical-ecological pathways that drive resistome amplification, for example through the design of low-interactivity polymers or signal-interference strategies.

The authors declare that they have no known competing financial interests or personal relationships that could have appeared to influence the work reported in this paper.

CRediT authorship contribution statement

Ruan Ruiqian: Methodology, Investigation, Data curation. **Tongyi Yang:** Writing – original draft, Methodology, Data curation, Conceptualization. **Jia Qianqian:** Writing – review & editing, Funding acquisition, Data curation, Conceptualization. **Yixuan Yang:** Writing – review & editing, Validation, Conceptualization. **Li-zhi Huang:** Software. **Huazhe Jiao:** Validation, Funding acquisition. **Zechong Guo:** Validation, Resources. **Haifeng Chen:** Validation. **Xiaona Dong:** Methodology. **Linzhi Zhai:** Methodology, Investigation. **Xiujie Wang:** Validation, Investigation.

Declaration of Competing Interest

The authors declare that they have no known competing financial interests or personal relationships that could have appeared to influence the work reported in this paper.

Acknowledgements

This work was financially supported by the National Natural Science Foundation of China (Grant No. 52374121; 32571895) and the Natural Science Foundation of Jiangsu Province (BK20251010).

Appendix A. Supporting information

Supplementary data associated with this article can be found in the online version at doi:10.1016/j.jhazmat.2026.141592.

Data availability

Data will be made available on request.

References

[1] Naghavi, M., Vollset, S.E., Ikuta, K.S., et al., 2024. Global burden of bacterial antimicrobial resistance 1990–2021: a systematic analysis with forecasts to 2050. Lancet 404, 1199–1226. https://doi.org/10.1016/s0140-6736(24)01867-1.
[2] Zhu, D., Ma, J., Li, G., Rillig, M.C., Zhu, Y.-G., 2021. Soil plastispheres as hotspots of antibiotic resistance genes and potential pathogens. ISME J 16, 521–532. https://doi.org/10.1038/s41396-021-01103-9.
[3] Forsberg, K.J., Reyes, A., Wang, B., Selleck, E.M., Sommer, M.O.A., Dantas, G., 2012. The shared antibiotic resistome of soil bacteria and human pathogens. Science 337, 1107–1111. https://doi.org/10.1126/science.1220761.
[4] Tang, K.H.D., Li, R., 2024. Aged Microplastics and antibiotic resistance genes: a review of aging effects on their interactions, 941–941 Antibiotics 13. https://doi.org/10.3390/antibiotics13100941.
[5] Sajjad, M., Huang, Q., Khan, S., Khan, M.A., Liu, Y., Wang, J., Lian, F., Wang, Q., Guo, G., 2022. Microplastics in the soil environment: A critical review, 102408–102408 Environ Technol amp Innov 27. https://doi.org/10.1016/j.eti.2022.102408.
[6] Aralappanavar, V.K., Mukhopadhyay, R., Yu, Y., Liu, J., Bhatnagar, A., Praveena, S. M., Li, Y., Paller, M., Adyel, T.M., Rinklebe, J., Bolan, N.S., Sarkar, B., 2024. Effects of microplastics on soil microorganisms and microbial functions in nutrients and carbon cycling – A review, 171435–171435 Sci Total Environ 924. https://doi.org/10.1016/j.scitotenv.2024.171435.
[7] Fred-Ahmadu, O.H., Bhagwat, G., Oluyoye, I., Benson, N.U., Ayejuyo, O.O., Palanisami, T., 2020. Interaction of chemical contaminants with microplastics: principles and perspectives. Sci Total Environ 706, 135978. https://doi.org/10.1016/j.scitotenv.2019.135978.
[8] Torres, F.G., Dioses-Salinas, D.C., Pizarro-Ortega, C.I., De-la-Torre, G.E., 2021. Sorption of chemical contaminants on degradable and non-degradable microplastics: recent progress and research trends. Sci Total Environ 757, 143875. https://doi.org/10.1016/j.scitotenv.2020.143875.
[9] Guo, X., Wang, X., Zhou, X., Kong, X., Tao, S., Xing, B., 2012. Sorption of four hydrophobic organic compounds by three chemically distinct polymers: role of chemical and physical composition. Environ Sci Technol 46 (13), 7252–7259. https://doi.org/10.1021/es301386z.
[10] Wang, F., Zhang, M., Sha, W., Wang, Y., Hao, H., Dou, Y., Li, Y., 2020. Sorption behavior and mechanisms of organic contaminants to nano and microplastics, 1827–1827 molecules 25. https://doi.org/10.3390/molecules25081827.
[11] Velzeboer, I., Kwadijk, C., Koelmans, A., 2014. Strong sorption of PCBs to nanoplastics, microplastics, carbon nanotubes, and fullerenes. Environ Sci Technol 48 (9), 4869–4876. https://doi.org/10.1021/es405721v.
[12] Wu, C., Zhang, K., Huang, X., Liu, J., 2016. Sorption of pharmaceuticals and personal care products to polyethylene debris. Environ Sci Pollut Res 23, 8819–8826. https://doi.org/10.1007/s11356-016-6121-7.
[13] Müller, A., Becker, R., Dorgerloh, U., Simon, F.-G., Braun, U., 2018. The effect of polymer aging on the uptake of fuel aromatics and ethers by microplastics. Environ Pollut 240, 639–646. https://doi.org/10.1016/j.envpol.2018.04.127.

[14] Bondareva, J.V., Rubekina, A.A., Maslakov, K.I., Demin, V.A., Timokhina, E.N., Astakhova, T.Yu, Kvashnin, D.G., Evlashin, S.A., 2026. Graphene oxide functionalization: Role of indole and imidazole in reduction and surface modification. Diam Relat Mater 161, 113113. https://doi.org/10.1016/j.diamond.2025.113113.
[15] Goveas, L.C., 2025. Interactions between polyaromatic hydrocarbons and microplastics: Environmental mechanisms and ecotoxicological impacts. Environ Geochem Health 47. https://doi.org/10.1007/s10653-025-02636-0.
[16] Iwamura, T., Okuzumi, S., Adachi, K., Takahashi, M., Shiotsuki, M., 2024. Direct evidence of π–π interactions in transparent organic–inorganic polymer hybrids of polystyrene and silica gel. Adv Polym Technol 2024, 1–6. https://doi.org/10.1155/2024/8362248.
[17] Bai, G., Wang, C., Wang, B., Promcharoen, P., Chumkaeo, P., Somsook, E., 2025. Sustainable adsorption of polystyrene microplastics in aqueous media using PET-C synthesized from plastic waste: DFT and experimental studies. ACS Sustain Chem Eng 13, 15792–15804. https://doi.org/10.1021/acssuschemeng.5c02073.
[18] Wang, H., Xu, K., Wang, J., Feng, C., Chen, Y., Shi, J., Ding, Y., Deng, C., Liu, X., 2023. Microplastic biofilm: An important microniche that may accelerate the spread of antibiotic resistance genes via natural transformation. J Hazard Mater 459, 132085. https://doi.org/10.1016/j.jhazmat.2023.132085.
[19] Han, J., Li, D., Zhang, M., Yu, X., Jia, X., Xu, H., Yan, X., Jia, W., Niu, S., Kempher, M.L., Tao, X., He, Y., 2020. *EmhR* is an indole-sensing transcriptional regulator responsible for the indole-induced antibiotic tolerance in *Pseudomonas fluorescens*. Environ Microbiol 23, 2054–2069. https://doi.org/10.1111/1462-2920.15354.
[20] Wu, T., Wilhelm, M.J., Li, Y., Ma, J., Dai, H.-L., 2022. Indole facilitates antimicrobial uptake in bacteria. ACS Infect Dis 8, 1124–1133. https://doi.org/10.1021/acsinfecdis.1c00618.
[21] Kim, J., Park, W., 2015. Indole: a signaling molecule or a mere metabolic byproduct that alters bacterial physiology at a high concentration? J Microbiol 53, 421–428. https://doi.org/10.1007/s12275-015-5273-3.
[22] Inaba, T., Obana, N., Habe, H., Nomura, N., 2020. Biofilm formation by *Streptococcus mutans* is enhanced by indole via the quorum sensing pathway. Micro Environ 35, 1–5. https://doi.org/10.1264/jsme2.me19164.
[23] Beaber, J., Hochhut, B., Waldor, M., 2004. SOS response promotes horizontal dissemination of antibiotic resistance genes. Nature 427, 72–74. https://doi.org/10.1038/nature02241.
[24] Amer, M.A., Ramadan, M.A., Attia, A.S., Wasfi, R., 2022. Silicone Foley catheters impregnated with microbial indole derivatives inhibit crystalline biofilm formation by Proteus mirabilis. Front Cell Infect Microbiol 12, 1–12. https://doi.org/10.3389/fcimb.2022.1010625.
[25] Ma, Q., Zhang, X., Qu, Y., 2018. Biodegradation and biotransformation of indole: Advances and perspectives. Front Microbiol 9, 1–18. https://doi.org/10.3389/fmicb.2018.02625.
[26] Zhang, J., Lu, K., Zhu, L., Li, N., Lin, D., Cheng, Y., Wang, M., 2023. Inhibition of quorum sensing serves as an effective strategy to mitigate the risks of human bacterial pathogens in soil. J Hazard Mater 465, 133272. https://doi.org/10.1016/j.jhazmat.2023.133272.
[27] Wang, M., Lian, Y., Wang, Y., Zhu, L., 2023. The role and mechanism of quorum sensing on environmental antimicrobial resistance. Environ Pollut 322, 121238. https://doi.org/10.1016/j.envpol.2023.121238.
[28] Seeley, M.E., Song, B., Passie, R., Hale, R.C., 2020. Microplastics affect sedimentary microbial communities and nitrogen cycling. Nat Commun 11, 1–10. https://doi.org/10.1038/s41467-020-16235-3.
[29] De Preter, C.C., Heinricher, M.M., 2024. Element cycling with micro(nano)plastics. Science 385, 933–935. https://doi.org/10.1126/science.adr5900.
[30] Kang, J., Ma, T., Zhou, Q., Gao, X., Chen, Y., Wu, J., Chen, J., Xiang, Y., 2015. New insight into DOC and DON in a drinking water biological aerated filter (BAF) by multimethod and correlation analysis of 3D-EEM. Anal Methods 7, 9885–9893. https://doi.org/10.1039/c5ay02156a.
[31] Li, L., Wang, Y., Zhang, W., Yu, S., Wang, X., Gao, N., 2019. New advances in fluorescence excitation-emission matrix spectroscopy for the characterization of dissolved organic matter in drinking water treatment: a review, 122676–122676 Chem Eng J 381. https://doi.org/10.1016/j.cej.2019.122676.
[32] Lin, D., Yang, G., Dou, P., Qian, S., Zhao, L., Yang, Y., Fanin, N., 2020. Microplastics negatively affect soil fauna but stimulate microbial activity: insights from a field-based microplastic addition experiment, 20201268–20201268 Proc R Soc B 287. https://doi.org/10.1098/rspb.2020.1268.
[33] Huang, Y., Zhao, Y., Wang, J., Zhang, M., Jia, W., Qin, X., 2019. LDPE microplastic films alter microbial community composition and enzymatic activities in soil. Environ Pollut 254, 112983. https://doi.org/10.1016/j.envpol.2019.112983.
[34] Qiu, X., Ma, S., Pan, J., Cui, Q., Zheng, W., Ding, L., Liang, X., Xu, B., Guo, X., Rillig, M.C., 2024. Microbial metabolism influences microplastic perturbation of dissolved organic matter in agricultural soils. ISME J 18, 1–12. https://doi.org/10.1093/ismejo/wrad017.
[35] Wilkes, R.A., Aristilde, L., 2017. Degradation and metabolism of synthetic plastics and associated products by*Pseudomonas*sp.: capabilities and challenges. J Appl Microbiol 123, 582–593. https://doi.org/10.1111/jam.13472.
[36] Lee, J.-H., Lee, J., 2010. Indole as an intercellular signal in microbial communities. FEMS Microbiol Rev 34, 426–444. https://doi.org/10.1111/j.1574-6976.2009.00204.x.
[37] Bianchi, T.S., Osburn, C., Shields, M.R., Yvon-Lewis, S., Young, J., Guo, L., Zhou, Z., 2014. Deepwater horizon oil in Gulf of Mexico waters after 2 years: transformation into the dissolved organic matter pool. Environ Sci Technol 48, 9288–9297. https://doi.org/10.1021/es501547b.
[38] Shakil, S., Tank, S.E., Kokelj, S.V., Vonk, J.E., Zolkos, S., 2020. Particulate dominance of organic carbon mobilization from thaw slumps on the Peel Plateau, NT: quantification and implications for stream systems and permafrost carbon release, 114019–114019 Environ Res Lett 15. https://doi.org/10.1088/1748-9326/abac36.
[39] He, W., Hur, J., 2015. Conservative behavior of fluorescence EEM-PARAFAC components in resin fractionation processes and its applicability for characterizing dissolved organic matter. Water Res 83, 217–226. https://doi.org/10.1016/j.watres.2015.06.044.
[40] Jia, W., Karapetrova, A., Zhang, M., Xu, L., Li, K., Huang, M., Wang, J., Huang, Y., 2022. Automated identification and quantification of invisible microplastics in agricultural soils. Sci Total Environ 844, 156853. https://doi.org/10.1016/j.scitotenv.2022.156853.
[41] Wang, P.-Y., Zhao, Z.-Y., Xiong, X.-B., Wang, N., Zhou, R., Zhang, Z.-M., Ding, F., Hao, M., Wang, S., Ma, Y., Uzamurera, A.G., Xiao, K.-W., Khan, A., Tao, X.-P., Wang, W.-Y., Tao, H.-Y., Xiong, Y.-C., 2023. Microplastics affect soil bacterial community assembly more by their shapes rather than the concentrations, 120581–120581 Water Res 245. https://doi.org/10.1016/j.watres.2023.120581.
[42] Dai, C., Ma, F., Wu, W., Li, S., Yang, J., Chen, Z., Lian, S., Qu, Y., 2023. Metagenomic analysis reveals indole signaling effect on microbial community in sequencing batch reactors: quorum sensing inhibition and antibiotic resistance enrichment. Environ Res 229, 115897. https://doi.org/10.1016/j.envres.2023.115897.
[43] Kim, J., Kim, T.-H., Park, S.R., Lee, H.J., Kim, J.K., 2020. Factors controlling the distributions of dissolved organic matter in the East China Sea during summer. Sci Rep 10, 1–10. https://doi.org/10.1038/s41598-020-68863-w.
[44] Fouché, J., Christiansen, C.T., Lafrenière, M.J., Grogan, P., Lamoureux, S.F., 2020. Canadian permafrost stores large pools of ammonium and optically distinct dissolved organic matter. Nat Commun 11, 1–11. https://doi.org/10.1038/s41467-020-18331-w.
[45] Zhu, Y.-G., Johnson, T.A., Su, J.-Q., Qiao, M., Guo, G.-X., Stedtfeld, R.D., Hashsham, S.A., Tiedje, J.M., 2013. Diverse and abundant antibiotic resistance genes in Chinese swine farms. Proc Natl Acad Sci USA 110, 3435–3440. https://doi.org/10.1073/pnas.1222743110.
[46] Chaudhary, M.K., Jadhav, I., Banjara, M.R., 2023. Molecular detection of plasmid mediated *blaTEM*, *blaCTX−M*,and *blaSHV* genes in Extended Spectrum β-Lactamase (ESBL) *Escherichia coli* from clinical samples. Ann Clin Microbiol Antimicrob 22, 1–7. https://doi.org/10.1186/s12941-023-00584-0.
[47] Yang, T., Zhai, D., Ding, X., Guo, Z., Zhao, Y., 2023. Shifts in soil microbial diversity and functions during continuous cropping of strawberry. Land Degrad Dev 34, 4810–4820. https://doi.org/10.1002/ldr.4811.
[48] Hu, H.-W., Wang, J.-T., Li, J., Shi, X.-Z., Ma, Y.-B., Chen, D., He, J.-Z., 2016. Long-term nickel contamination increases the occurrence of antibiotic resistance genes in agricultural soils. Environ Sci Technol 51, 790–800. https://doi.org/10.1021/acs.est.6b03383.
[49] Wang, W., Yao, S., Zhao, Z., Liu, Z., Li, Q.X., Yan, H., Liu, X., 2023. Degradation and potential metabolism pathway of polystyrene by bacteria from landfill site. Environ Pollut 343, 123202. https://doi.org/10.1016/j.envpol.2023.123202.
[50] Wang, Y.-F., Liu, Y.-J., Fu, Y.-M., Xu, J.-Y., Zhang, T.-L., Cui, H.-L., Qiao, M., Rillig, M.C., Zhu, Y.-G., Zhu, D., 2024. Microplastic diversity increases the abundance of antibiotic resistance genes in soil. Nat Commun 15, 9788. https://doi.org/10.1038/s41467-024-54237-7.
[51] Lin, L., Zhang, X., Yuan, B., Li, H., Lu, H., Liu, J., Hong, H., Yan, C., 2023. Effects of biofouling on the properties and sinking behavior of disposable face masks in seawater: a systematic comparison with microplastic films and particles. Environ Sci Technol Lett 10, 792–797. https://doi.org/10.1021/acs.estlett.3c00460.
[52] Fu, L., Li, J., Wang, G., Luan, Y., Dai, W., 2021. Adsorption behavior of organic pollutants on microplastics, 112207–112207 Ecotoxicol Environ Saf 217. https://doi.org/10.1016/j.ecoenv.2021.112207.
[53] Yang, T., Yuan, R., Zou, X., Dai, M., Dong, X., Chen, H., Guo, Z., Jiao, H., Yang, Y., 2025. Indole-mediated reconfiguration of soil microbial consortia in response to microplastic pollution. J Environ Chem Eng 13, 115961. https://doi.org/10.1016/j.jece.2025.115961.
[54] Wang, Y., Li, H., Cui, X., Zhang, X.-H., 2017. A novel stress response mechanism, triggered by indole, involved in quorum quenching enzyme MomL and iron-sulfur cluster in *Muricauda olearia* Th120. Sci Rep 7, 1–10. https://doi.org/10.1038/s41598-017-04606-8.
[55] Pons, M.C., Praud, K., Da Re, S., Cloeckaert, A., Doublet, B., 2022. Conjugative IncC plasmid entry triggers the SOS response and promotes effective transfer of the integrative antibiotic resistance element SGI1. Microbiol Spectr 11, 1–13. https://doi.org/10.1128/spectrum.02201-22.
[56] Zabłotni, A., Schmidt, M., Siwińska, M., 2024. The SOS response activation and the risk of antibiotic resistance enhancement in *Proteus spp.* strains exposed to subinhibitory concentrations of ciprofloxacin, 119–119 Int J Mol Sci 26. https://doi.org/10.3390/ijms26010119.
[57] Latha, K., Lalithakumari, D., 2001. Transfer and expression of a hydrocarbon-degrading plasmid pHCL from *Pseudomonas putida* to marine bacteria. World J Microbiol Biotechnol 17, 523–528. https://doi.org/10.1023/a:1011917408368.
[58] Romdhane, S., Spor, A., Aubert, J., Bru, D., Breuil, M.-C., Hallin, S., Mounier, A., Ouadah, S., Tsiknia, M., Philippot, L., 2021. Unraveling negative biotic interactions determining soil microbial community assembly and functioning. ISME J 16, 296–306. https://doi.org/10.1038/s41396-021-01076-9.
[59] Foster, K.R., Bell, T., 2012. Competition, not cooperation, dominates interactions among culturable microbial species. Curr Biol 22, 1845–1850. https://doi.org/10.1016/j.cub.2012.08.005.

[60] Zhou, R., Huang, X., Xie, Z., Ding, Z., Wei, H., Jin, Q., 2024. A review focusing on mechanisms and ecological risks of enrichment and propagation of antibiotic resistance genes and mobile genetic elements by microplastic biofilms, 118737–118737 Environ Res 251. https://doi.org/10.1016/j.envres.2024.118737.
[61] Ruan, C., Ramoneda, J., Gogia, G., Wang, G., Johnson, D.R., 2022. Fungal hyphae regulate bacterial diversity and plasmid-mediated functional novelty during range expansion. Curr Biol 32, 5285–5294.e4. https://doi.org/10.1016/j.cub.2022.11.009.
[62] Nazir, R., Shen, J.-P., Wang, J.-T., Hu, H.-W., He, J.-Z., 2017. Fungal networks serve as novel ecological routes for enrichment and dissemination of antibiotic resistance genes as exhibited by microcosm experiments. Sci Rep 7, 15457. https://doi.org/10.1038/s41598-017-15660-7.
[63] Nazir, R., Du, S., Shen, J.-P., Hu, H.-W., Wang, J.-T., He, J.-Z., 2024. Effect of meddling ARBs on ARGs dynamics in fungal infested soil and their selective dispersal along spatially distant mycelial networks, 174594–174594. Sci Total Environ 947. https://doi.org/10.1016/j.scitotenv.2024.174594.
[64] Deng, W., Wang, Y., Fu, M., Wang, Z., Di, X., Wang, J., Liu, W., 2025. The spatiotemporal successions of bacterial and fungal plastisphere communities and their effects on microplastic degradation in soil ecosystems. Environ Sci Technol 59, 15408–15419. https://doi.org/10.1021/acs.est.5c06662.
[65] Wang, C., Kuzyakov, Y., 2024. Mechanisms and implications of bacterial-fungal competition for soil resources. ISME J 18, 1–18. https://doi.org/10.1093/ismejo/wrae073.
[66] Rillig, M.C., Kim, S.W., Zhu, Y.-G., 2023. The soil plastisphere. Nat Rev Microbiol 22, 64–74. https://doi.org/10.1038/s41579-023-00967-2.